

The VSOP 5-GHz AGN Survey: IV. The Angular Size/Brightness Temperature Distribution

S. Horiuchi¹

Jet Propulsion Laboratory, Pasadena, CA 91109, USA

shoriuchi@swin.edu.au

E. B. Fomalont

National Radio Astronomy Observatory, Charlottesville, VA 22903, USA

efomalon@nrao.edu

W. K. Scott A. R. Taylor

University of Calgary, Calgary, Canada

bill@ras.ucalgary.ca, russ@ras.ucalgary.ca

J. E. J. Lovell

Australia Telescope National Facility, Canberra, Australia

Jim.Lovell@csiro.au

G. A. Moellenbrock

National Radio Astronomy Observatory, Socorro, NM 87801

gmoellen@nrao.edu

R. Dodson, Y. Murata, H. Hirabayashi & P. G. Edwards

*Institute of Space and Astronautical Science, Japan Aerospace Exploration Agency Kanagawa 229-8510,
Japan*

rdodson@vsop.isas.jaxa.jp, murata@vsop.isas.jaxa.jp, hirax@vsop.isas.jaxa.jp,
pge@vsop.isas.jaxa.jp

L. I. Gurvits

Joint Institute for VLBI in Europe, Dwingeloo, The Netherlands

lgurvits@jive.nl

Z-Q. Shen

Shanghai Astronomical Observatory, Chinese Academy of Sciences, Shanghai 200030, China

zshen@shao.ac.cn

Subject headings: AGN: radio, quasar—VLBI: survey

ABSTRACT: The VSOP (VLBI Space Observatory Programme) mission is a Japanese-led project to study radio sources with sub-milliarcsec angular resolution, using an orbiting 8-m telescope on board the satellite HALCA with a global earth-based array of telescopes. A major program is the 5 GHz VSOP Survey Program, which we supplement here with VLBA observations to produce a complete and flux-density limited sample. Using statistical methods of analysis of the observed visibility amplitude versus projected (u,v) spacing, we have determined the angular size and brightness temperature distribution of bright AGN radio cores. On average, the cores have a diameter (full-width, half-power) of 0.20 mas which contains about 20% of the total source emission, and $14 \pm 6\%$ of the cores are < 0.04 mas in size. About $20 \pm 5\%$ of the radio cores have a source frame brightness temperature $T_b > 1.0 \times 10^{13}$ K, and $3 \pm 2\%$ have $T_b > 1.0 \times 10^{14}$ K. A model of the high brightness temperature tail suggests that the radio cores have a brightness temperatures $\approx 1 \times 10^{12}$ K, and are beamed toward the observer with an average bulk motion of $\beta = 0.993 \pm 0.004$.

1. Introduction

On 1997 February 12, the Institute of Space and Astronautical Science of Japan (ISAS) launched a satellite called HALCA, with an 8-m radio telescope dedicated exclusively to Very Long Baseline Interferometry (VLBI) (Hirabayashi et al. 1998). The mission, called VSOP, with a spacecraft apogee height of 21400 km, gives unparalleled brightness temperature sensitivity, and allows studies of radio sources with angular resolution as small as 0.2 mas. About 75% of the mission observing time was devoted to peer-reviewed scientific projects, proposed by the world-wide astronomical community (called General Observing Time, GOT). Many VSOP publications show the complexity and evolution of the sub-milliarcsec structure of AGNs (Piner et al. 2000; Lobanov & Zensus 2001; Lister et al. 2001a; Tingay et al. 2002; Kameno et al. 2003; Murphy et al. 2003; Giroletti et al. 2004).

In order to insure that a complete flux-density limited sample of AGNs were observed during the

¹Present address: Swinburne University of Technology, Hawthorn, Vic. 3122, Australia

observing lifetime, the mission-led part, the VSOP 5-GHz AGN Survey, was given a major portion of the remaining observing time for sources which were not already included in GOT proposals. A general goal of the survey is a compilation of a catalog of AGN which would be used in part for planning for future space VLBI missions. A more immediate goal, reported in this paper, is to characterize the properties of the sub-milliarcsec structure in AGN, especially their angular size and brightness temperature distributions.

This paper, the fourth in the VSOP AGN Survey series, presents a non-imaging statistical analysis of the angular size and brightness temperature distributions of strong AGNs. This is complementary to the approach in Paper III Scott et al. (2004) which shows the images, model fits, angular sizes and bright temperatures for 102 sources. A description of the survey compilation and supporting VLBA observations was given in Paper I by Hirabayashi et al. (2000), with additional material in Fomalont et al. (2000a). The VSOP observations and data reductions are described in Paper II by Lovell et al. (2004) (see also Moellenbrock et al. (2000)). In §2, we discuss the source selection and in §3 describe how the observed visibility amplitude versus projected spacing was determined in order to obtain a statistic which could be used to determine the angular size properties of AGN. In §4, we derive the angular size and brightness temperature distributions. We compare them with other high resolution surveys and scintillation observations, and fit a simple model to the distributions. The major results are summarized in §5.

2. Compilation of the Data-Base

2.1. The VSOP AGN Survey Sample

The VSOP 5 GHz AGN sample (Hirabayashi et al. 2000) was defined to include all cataloged extragalactic, flat-spectrum radio sources in the sky with

- a total flux density at 5 GHz, $S \geq 0.95$ Jy
- a spectral index $\alpha \geq -0.50$ ($S \propto \nu^\alpha$)
- a galactic latitude $|b| \geq 10^\circ$.

This sample contains 344 sources. This spectral index criterion eliminated from consideration about 300 extragalactic sources with flux density > 1 Jy near the galactic plane, or with steep radio spectra and thus little milliarcsec structure. These

sources are arcseconds in size and dominated by double-lobed structures (eg. FRI and FR II type radio sources) and are generally associated with radio galaxies. At the beginning of 2002 when this database was assembled, about 50% of the VSOP observations had been observed and processed. Because the selection of observed sources was randomized by the need to fill in observing holes between the GOT observations, little bias is introduced by not completing the observations of the entire list (See Fig. 1 of Paper III) before this analysis of the data.

An integral part of the planning for the VSOP Survey was VLBA observations over a 24-hour period in 1996 June, call the VLBA pre-launch survey (VLBApl). All 303 sources of the 344 sample sources north of declination -43° were observed at 5 GHz, and the survey results are given by Fomalont et al. (2000b)². The VLBApl survey served two important functions for the VSOP Survey. First, the VLBA results, with baselines up to 8000 km, indicated which of the AGN are sufficiently large so that higher resolution VSOP observations on baselines between 5000 km and 25000 km were not feasible. Secondly, when combined with the VSOP data, this enhanced database covers baselines between 100 km and 25000 km so that a detailed analysis over a large range of the angular structure of AGNs could be made. Although the VLBA data were implicitly used in Paper III in order to obtain VSOP images which were consistent with the lower resolution data, direct use of the VSOP+VLBA data provides a more accurate determination of the sub-milliarcsec properties of AGNs, less susceptible to selection effects, observational biases and the present incompleteness of the observations.

2.2. Determining the Visibility Database

The observational procedures and data reduction techniques for the survey experiments are given in Papers II and III. After calibration and editing, the basic database for each source is composed of a set of correlated visibilities (amplitude and phase), measured at many (u,v) spacings. Numerous examples of the character of the data are given in Fig. 2 of Paper III. For many of the survey observations only two or three ground telescopes

with HALCA for three or four hours were used. The large variation of the observation time and ground telescope participation produced a set of images with a wide range of quality and resolution, and direct analysis of them can lead to uncertainties in determining the unbiased properties of AGNs. Thus, our statistical analysis uses the visibility data directly in order to determine the AGN distribution of angular size and brightness temperature.

In order to extend the range of resolution of the data, we concatenated the VSOP data and the VLBApl data, and for this reason we have restricted the analysis to the 303 survey sources north of declination -43° which is covered by the VLBA observations. In Fig. 1 we give an example of the concatenated data set for J1626–2951 and relevant processing. Fig. 1a shows the visibility amplitude versus the projected (u,v) spacing for the VSOP data observed on 22 February 1998, plus the VLBA data observed on 05 June 1996. The effect of the source variability is obvious since the VLBA points which overlap in spacing with the VSOP points are considerably higher. Using the flux density monitoring of the sources with the Australia Telescope Compact Array (ATCA) (Tingay et al. 2003), we find that the flux density of this source in June 1996 was 3.0 Jy, but only 2.1 Jy in February 1998. Although the variable component in most AGN are confined to a small region of the emission extent, the overlap in spacing and position angle between the VLBA and VSOP surveys are sufficient to compare their visibility amplitude. In the example of Fig. 1a, if the VLBA amplitude scale is multiplied by 2.1/3.0, a better continuity between the VLBA and VSOP points, as shown in Fig. 1b, is obtained. (The large change in flux density for this source is atypical.) Source variability corrections to an accuracy of 10% were obtained from the ATCA and University of Michigan³ source monitoring programs which include most of the sources in the VSOP sample. Finally, in order to decrease the size of the database, we averaged the observed visibility amplitude in bins of width $40 M\lambda$, and this plot is shown in Fig. 1c. With the above processing, we obtained a database containing the visibility amplitude over a wide range of projected spacing for

²<http://www.aoc.nrao.edu/vlba/html/6CM/index.htm>

³<http://www.astro.lsa.umich.edu/obs/radiotel/umrao.html>

all sources.

The VSOP Survey source list of the 303 sources north of declination -43° is given in Table 1. It is arranged as follows:

Columns 1 and 2 give the J2000 name, and an alternative name.

Column 3 lists the total flux density of the source at 5 GHz. Most of the sources are variable and the total flux density comes from that of the original finding catalog, as described in (Hirabayashi et al. 2000), or from the VLBA observations.

Column 4 gives the optical identification: q=quasar, e=elliptical galaxy, g=faint galaxy (> 24 mag), b=BLLac object, e=empty field.

Column 5 gives the redshift, if available. Many come from the NASA/IPAC Database (NED, <http://nedwww.ipac.caltech.edu>)

Column 6 gives the VSOP observation code. For additional information for any source, see the VSOP Survey Program website⁴.

Column 7 gives the status of the survey observation. Class A (115 sources) means that the VSOP data for the source have been completely processed and are used in this analysis. Class B (124 sources) means that the VSOP data for the source are not yet available. Class C (50 sources) are in the VSOP AGN sample, but were so resolved in the VLBA observations, they were not included as VSOP targets. However, they are included as representative of low brightness objects in the statistical analysis. Class D (14 sources) are so resolved with the VLBApl, that they have been removed from the VSOP AGN sample as far as the statistical analysis is concerned.

Column 8 gives the approximate brightness temperature for sources observed with VSOP. These are calculated by taking the correlated flux density at the longest spacing observed for the source, which is then converted to brightness temperature in units of 10^{12} K.

These values are meant solely to be an indication of which sources have a component of high brightness temperature. Refer to Paper III for a more exact determination of the brightness temperature of source components. The approximate brightness temperature here has been used in later discussions.

Column 9 gives the date of the VSOP observations in day-month-year format.

Column 10 gives the data of the VLBA observation in day-month-year format. Most were obtained on 05 June 1996 from the VLBApl survey. VSOP survey data extracted from the VSOP general observing time observations which used the VLBA have the same date as the VSOP observation.

Column 11 indicates with an 'M' if the source is included in the 15 GHz Monitoring Of Jets in Active galaxies with VLBA Experiments (MOJAVE program)⁵.

3. The Relative Visibility versus Projected Spacing

The data for all sources were processed to that of the form given in Fig. 1c. In order to have a statistic which is independent of the total flux density of the source, we normalized the measured correlated flux density of each source to the average visibility amplitude in the first bin of average spacing $20 M\lambda$. We will denote this normalized flux density as the relative visibility (RV) and it is a property of the source structure, regardless of the total intensity of the source. The properties of the RV with projected (u,v) spacing (PS) is the statistic that are used to categorize the source structure properties of AGN.

In order to determine an unbiased RV versus PS distribution, we averaged the contributions of the 303 sources in the following manner. First, we included the 115 fully-reduced sources, Class=A, 48.1% of the sample. We contend that those sources not yet observed or reduced, Class=B, have the same average properties of those in Class=A. We included a representative portion of the 50 sources (Class = C) which were too resolved to be observed with HALCA but are

⁴http://www.jaxa.jp/survey/survey_db.html

⁵<http://www.physics.purdue.edu/~mlister/MOJAVE/>

nevertheless part of the VSOP AGN Sample. In practice we choose all 50, but reduced their weight in the analysis to 0.481 to match the portion of VSOP observations which have been observed and reduced by 2002 February.

Fig. 2 shows the dependence of the average RV versus PS for the sample. Although data from 165 sources of the 303 in the sample are included, the distribution should be representative of the entire sample, as described above. A preliminary version of this distribution, with fewer sources, was presented by Lovell et al. (2000). The distribution shows a strong decrease between 20 M λ and 140 M λ , with a less steep decrease at longer spacings. At 500 M λ , the RV is 20% of that at 20 M λ . Based on the measured total flux density of the sources (see Table 1, col 3) the visibility amplitude at the first point at 20 M λ is, on average, only 52% of the total source flux density at zero projected spacing. Thus, a typical AGN contains about half of its emission in angular scales > 10 mas which is invisible in the VLBA and VSOP observations, but contained in the total source flux density.

For comparison, the distribution from the VSOP observations of the Pearson-Readhead (PR) sample at 5 GHz (Lister et al. 2001a) is also shown in Fig. 2. This sample of 27 sources is defined by $\delta > 35^\circ$, total flux density > 1.3 Jy, with correlated flux density > 0.4 Jy on a 6000 km (100 M λ) baseline. Using the same visibility amplitude normalization as that used with the VSOP Survey sample, the PR distribution is in reasonable agreement with that found with the VSOP sample. For the PR sample, there is smaller decrease of the RV for the longer spacings since the sample definition included a criterion concerning the compactness of a source.

The distribution of the RV versus PS can be interpreted as that produced by a typical AGN structure. We have, thus, fit this distribution to an average source structure, given by the dashed line in Fig. 2. For the space baselines of $PS > 180$ M λ , the distribution can be fit with a component of angular size 0.20 ± 0.02 mas, containing $0.40 \pm 0.04\%$ of the mas-scale flux density, or about 20% of the total flux density. The fit to shorter spacings is more ambiguous, and a range of angular scale components are needed. Most of the emission is contained in an ≈ 1 mas-sized component, but some

emission is required in a component of ≈ 2.4 mas to fit the shortest VLBA spacings. As described above, a typical AGN contains even more extended emission with a scale size > 10 mas which is unobservable with the VLBA or VSOP, but have been imaged with lower frequency VLBI surveys.

The fit in Fig. 2 of the three components with different angular scales is consistent with the known structure of many AGNs: The smallest angular component is the radio core which is generally less than 1 mas in size. This component is associated with the inner part of the radio jet which is often beamed toward the observer. The two larger components are consistent with the radio jet and internal structures observed in many sources. The radio emission, which is completely resolved out in these observations, is associated with larger-scale kpc-size emission. Since the structure of most radio sources is asymmetric with the radio core at one end of a linear structure, we originally fit the data in Fig. 2 to an asymmetric spatial distribution of the three components. However, the fitting is insensitive to source asymmetry, but depends strongly on the component angular scales.

4. The Statistical Properties of Radio Cores

4.1. The Angular Size Distribution

Each plotted point in Fig. 2 represents the average RV for the set of sources. By fitting this RV distribution to a typical AGN source model, we obtained an average source structure. In Fig. 3 we show the range of values for the RV associated with three spacings; 60 M λ , 220 M λ and 440 M λ , and the spread of these values is related to the distribution of the angular size of the AGN population. At the shortest spacing of 60 M λ , about 60% of the sources are nearly unresolved ($RV > 0.8$), and about 12% of the sources have $RV < 0.4$. At the long spacing of 440 M λ , nearly 40% of the sources have $RV < 0.2$, and only about 30% have $RV > 0.4$.

In order to determine the range of source sizes which are consistent with the distributions in Fig. 3, we used the template structure of the three-component average source model. In other words, we assumed that all sources have the same shape RV versus PS, but are scaled in angular size (or

spacing). We then convolved this template structure with a two-parameter log-normal distribution $P(\theta)$, where θ is the angular size of the radio core,

$$P(\theta)d\theta \propto \exp - \left(\frac{\log(\theta/\theta_l)}{d} \right)^2 d\theta, \quad (1)$$

with parameters θ_l , the log-mean of the angular size distribution, and d , the dispersion in the log of the angular size. The best fit for these two parameters was obtained by minimizing the χ^2 difference between the observed distribution in Fig. 3 with that expected from the template structure model, convolved with the distribution in Eq. (1). The result of this fit is a core size of $\theta_l = 0.052$ mas and dispersion $d = 1.45$, and the fit is shown by the dark plotted points in Fig. 3. The error bars represent the estimated error based on the number of sources used in each spacing range.

The cross-hatched histogram in Fig. 4 shows the angular size distribution for this fit. Approximately 80% of the radio sources have a core angular size in the range 0.03 mas to 0.8 mas. (The two larger radio components follow the same distribution, but are 5 and 12 times larger than the core.) About 14% and 4% of the sources may have an angular size less than 0.06 mas and 0.04 mas, respectively. Although the smaller angular sizes are clearly beyond the resolution capabilities of these observations of about 0.15 mas for the stronger cores (Paper III), our assumption of reasonable continuity in the distribution of angular sizes, implied by the use of Eq. (1), does infer that these small angular size components are likely to exist.

We also fit the RV vs PS distribution in Fig. 3 with an angular size model which attempts to minimize the number of small sources. The fainter, circle points show a fit to the data with parameters $\theta_l = 0.09$ mas and $d = 1.08$. These values produce an additional χ^2 deviation from the data which makes this solution (or a more extreme one) less than 15% as likely as a solution closer to the best model. This angular distribution limit is shown by the open histogram in Fig. 4, where it is referred to as ‘largest core’. For this distribution, the proportion of sources with cores with an angular diameter less than 0.06 mas has dropped from 14% to 6%, with only 1% less than 0.04 mas. The difference between the two distributions is an indication of the model error.

4.2. The Brightness Temperature Distribution

The brightness temperature distribution of the core component in the observer’s frame, $T_b \propto S/\theta^2$, can be derived from the angular size distributions given in Fig. 4, and the average core flux density, S . To obtain this core flux density, Fig. 5a shows a similar distribution to that of Fig. 2, but with the y-axis as the correlated flux density, rather than the RV. We have divided the distribution into a low and a high redshift distribution, separated at $z = 0.8$ which is the redshift median value for the sample. Thus, the core component, which becomes dominant at spacings greater than 300 M λ , has an average flux density of 0.5 Jy. The dependence of the core flux density with redshift is small, so that the assumption of converting the angular size distribution to a brightness temperature distribution using a well-defined average core flux density of 0.5 Jy is valid.

The brightness temperature distributions in the observer’s reference frame are shown in Fig. 6, for the best-fit angular size distribution and the ‘large-core’ angular distribution. About 14% of the sources have $T_b > 1.0 \times 10^{13}$ K for the best fit angular size distribution; whereas only 6% are above this temperature for the large-core fit. For both distribution, approximately half of all AGN have a radio core with $T_b > 1.0 \times 10^{12}$ K. These distributions agree well with that in Paper III derived from the images. Because our data modeling does not contain rigid cutoffs at the high resolution limit of the observations, but uses a reasonable extrapolation below the formal resolution limit the VSOP observations, the distributions in Fig. 6 extended to higher brightness temperatures than that from other VLBI surveys of AGN. Our addition of AGN which were not observed with VSOP because of the lack of significant small-scale structure also extends the brightness temperature distributions to lower values than other VLBI surveys.

To correct the brightness temperature T_b from the observer to the source reference frame, the factor $(1 + z)$, where z is the source redshift, should be applied to the brightness temperature. Fig. 5b shows the redshift distribution of the 267 sources in the sample with measured redshifts. The distribution is relatively flat out to $z = 1.5$, and

then drops off with a maximum redshift somewhat less than 3.0 for this sample. The average value of $(1+z)$ is 1.81. The plot in Fig. 5c shows a comparison of the approximate source brightness temperatures given in Table 1, col (8) versus redshift. There is clearly little systematic dependence of the brightness temperature with redshift, hence a simple multiplication of the brightness temperature scale in Fig. 6 by 1.81 converts from the observer frame to the source frame. This assumption should produce an error no larger than the 15% difference in the average core flux density for high and low brightness sources, as shown in Fig. 5a.

We believe that the statistical analysis of the VSOP+VLBA observations gives the most realistic and unbiased estimate of the proportion of high brightness radio cores at 5 GHz yet available. In the source reference frame approximately 25% of the radio cores have $T_b > 1.0 \times 10^{13}$ K using the best fit angular size distribution, but this proportion drops to 16% for the largest core angular size distribution. The proportion of the core with $T_b > 1.0 \times 10^{14}$ K is 4% and 1% for the two distributions. This brightness temperature corresponds to a resolution which is a factor of 10 sharper than the observed VSOP data, but we believe the percentages are reliable. Approximately 65% of the radio cores have $T_b > 1.0 \times 10^{12}$ K.

The above results are consistent with other surveys of compact radio sources. In the 15-GHz observations of Kovalev et al. (2004), 18 of 160 sources (13%) have $T_b > 1.0 \times 10^{13}$ K and 46% have $T_b > 1.0 \times 10^{12}$ K. A 22 GHz survey (Moellenbrock et al. 1996) found a similar percentage of high brightness objects. Our percentage of cores with $T_b > 1.0 \times 10^{12}$ K is in reasonable agreement (as it should be since the data overlap is large) with the 53% found by Scott et al. (2004) from the images and model-fitting of 102 sources from the VSOP Survey⁶. The highest brightness temperatures that has been measured for an individual source is 5.8×10^{13} K for AO0235+164 at 5 GHz (Frey et al. 2000).

The scintillation of many radio sources also implies that they contain radio components with

$T_b > 10^{14}$ K (Kedziora-Chudczer et al. 2001). Of the 710 sources surveyed with the VLA at 4.9 GHz, the Micro-Arcsecond Scintillation-Induced Variability Survey (MASIV) (Lovell et al. 2003), about 12% were classified as variable. The variability in the total flux density averaged about 6%, and that the variable time scales varied from a few hours to a few days. An approximate interpretation of these results is: about 12% of the AGNs contain a radio component with 6% of the total source flux density and $T_b \geq 10^{14}$ K. The results from our statistical analysis suggests that about 20% of the AGNs contain a radio component with 20% of the total source flux density and $T_b \geq 10^{13}$ K. These two descriptions of the properties of the high brightness radio cores are compatible. Finally, a correlation between sources which scintillate and those which have relatively large correlated flux density observed by VSOP was reported by Lister, Tingay & Preston (2001b) using the PR sample of sources. The detailed study of the scintillation properties of the VSOP sample is in progress.

4.3. Brightness Temperature Modeling

It is generally assumed that the maximum brightness temperature from a synchrotron emitting radio source is $T_{max} \approx 10^{12}$ K, because the strong inverse-Compton emission will quickly quench the radio emission above this brightness (Kellermann & Pauliny-Toth 1969; Lister et al. 2001a; Tingay et al. 2001; Kellermann 2002). Calculations based on equipartition of energy arguments suggest that this limit may be as low as $10^{10.5}$ K (Readhead et al. 1996). Other emission mechanisms have also been proposed, including relativistic induced Compton scattering (Sincell & Krolik 1994) and coherent synchrotron emission processes (Melrose 2002), which have a higher brightness temperature limit. The observed brightness temperatures above T_{max} , however, can be produced by the Doppler boosting (Shklovsky 1963) of the emission from the radio core material which moves with a relativistic bulk velocity v_b nearly in the direction to the observer, given by the angle, ψ .

In order to obtain estimates of the three parameters, T_{max} , $\beta = v_b/c$ and ψ needed to reproduce the high brightness tail of the distribution in Fig. 6, we used the following simple model: The

⁶Twenty sources in the Scott sample are not included in this statistical analysis because they were south of $\delta < -43$, or not within the strict definition of the catalog completeness. About 30 additional sources, with good visibility data, but not yet imaged, are included this statistical analysis.

number density of the source brightness temperature, $T < T_{max}$, is proportional to $\log(T_{max}/T)$; the motion of this material is β , and the maximum orientation to the line of sight is ψ . For a more detailed modeling of superluminal sources, see Vermeulen & Cohen (1994). The plotted points in Fig. 6 are those for the values $T_{max} = 1.0 \times 10^{12}\text{K}$, $\beta = 0.993$, $\psi = 35^\circ$. Reasonable fits are obtained for the range $0.5 < T_{max} < 2.0$ and $0.990 < \beta < 0.997$. Similar model parameters are obtained from multi-epoch observations of the ‘superluminal’ motions of radio components, which suggest $\beta \approx 0.99$, corresponding to $\gamma = (1 - \beta^2)^{-0.5} \approx 10$ (Vermeulen & Cohen 1994; Kellermann et al. 2000; Kovalev et al. 2004).

5. Conclusions

Before the launch of HALCA, there was little *direct* evidence concerning the brightness temperature distribution of radio components associated with AGN. Figs. 2 and 3 show that at 5 GHz with baselines up to 25,000 km there is significant emission for many AGNs, and future use of a space-VLBI mission with substantially longer baselines are required to probe the evolution and structure of these high brightness radio cores. Future space VLBI missions with longer baselines and substantially improved sensitivity are, thus, required to probe the evolution and structure of these high brightness cores in AGNs.

The VSOP AGN Survey was compiled in order to determine the properties of the sub-mas radio structure of strong AGN. The source sample covered the entire sky ($|b| > 10^\circ$) and included sources at 5 GHz above 1 Jy, with a relatively flat spectral index. No other criteria were used. The analysis in this paper provides an attempt at an unbiased determination of the radio source structure parameters by using the measured RV versus PS properties in a simple and straight-forward manner. An analysis from the derived images and models of the individual sources (Scott et al. 2004) obtains similar results on the angular size and brightness temperature of the AGNs.

The major properties of AGN derived from the statistical analysis described in this paper are:

- About 50% of the total emission from an average AGN is completely resolved using at the shortest VLBA spacings, and are there-

fore contained in a component > 10 mas in size.

- About 40% of the milliarcsec emission (20% of the total emission) comes from a radio core of average size 0.20 ± 0.02 mas.
- About 80% of the radio cores have an angular size in the range of 0.03 to 0.8 mas. We estimate that $10 \pm 4\%$ of the cores are < 0.06 mas at 5 GHz.
- A majority of the AGN radio cores have a brightness temperature in excess of 1.0×10^{12} K, and we estimate that $20 \pm 5\%$ of the cores have $T_b > 1.0 \times 10^{13}\text{K}$ and $3 \pm 2\%$ have $T_b > 1.0 \times 10^{14}\text{K}$ in the source reference frame.
- The derived brightness temperature distribution is in good agreement with the results from other high-resolution radio source surveys and with radio scintillation observations.

We gratefully acknowledge the VSOP project, which is led by the Institute of Space and Astronautical Science (ISAS, now called the Japan Aerospace Exploration Agency, JAXA) in cooperation with many organizations and radio telescopes around the world. The National Radio Astronomy Observatory is a facility of the National Science Foundation, operated under cooperative agreement by Associated Universities, Inc. SH acknowledges support through an NRC/NASA-JPL Research Associateship: WKS thanks the support from the Canadian Space Agency: RD is supported by the Japanese Society for the Promotion of Science: JEJL thanks the support from the Australian Commonwealth Scientific & Industrial Research Organisation. This research has made use of the NASA/IPAC Extragalactic Database (NED) which is operated by the Jet Propulsion Laboratory, California Institute of technology, under contract with the National Aeronautics and Space Administration. Finally, we thank an industrious referee for major improvements to the organization and content of the paper.

REFERENCES

Fomalont, E., et al. 2000a, in Proceedings of the VSOP Symposium, January 2000, Astrophys-

- ical Phenomena Revealed by Space VLBI, ed H. Hirabayashi, P. G. Edwards, & D. W. Murphy (Sagamihara: The Institute of Space and Astronautical Science), 167
- Fomalont, E. B., Frey, S., Paragi, Z., Gurvits, L. I., Scott, W. K., Taylor, A. R., Edwards, P. G., & Hirabayashi, H. 2000b, *ApJS*, 131, 95
- Frey, S., Gurvits, L. I., Altschuler, D. R., Davis, M. M., Perillat, P., Salter, C. J., Aller, H. D., Aller, M. F. & Hirabayashi, H. 2000, *PASA*, 52, 975
- Giroletti, M., Giovannini, G., Feretti, L., Cotton, W.D., Edwards, P.G., Lara, L., Marscher, A.P., Mattox, J.R., Piner, B.G. & Venturi, T. *ApJ*, 600, 127
- Heidt, J., Tröller, M., Nilsson, K., Jäger, K., Takalo, L., Rekola, R., & Sillanpää, A. 2004, *A&A*, 418, 813
- Hirabayashi, H., et al. 1998, *Science*, 281, 1825
- Hirabayashi, H., Fomalont, E., Horiuchi, S., et al. 2000, *PASA*, 52, 997, (Paper I)
- Kameno, S., Inoue, M., Wajima, Sawada-Satoh, S. & Shen, Z.-Q. 2003, *Publ of Astron Soc. of Australia*, 20, 134
- Kedziora-Chudczer, L. L., Jauncey, D. L., Wieringa, M. H., Tzioumis, A. K & Reynolds, J. E. 2001, *MNRAS*, 325, 1411
- Kellermann, I. I. & Pauliny-Toth, I. I. K. 1969, *ApJ*, 165, L71
- Kellermann, K. I., Vermeulen, R. C., Zensus, J. A. & Cohen, M. H. 2000, in *Proceedings of the VSOP Symposium, January 2000, Astrophysical Phenomena Revealed by Space VLBI*, ed H. Hirabayashi, P. G. Edwards, & D. W. Murphy (Sagamihara: The Institute of Space and Astronautical Science), 159
- Kellermann, K. I. 2002, *PASJ*, 19, 77
- Kovalev, Y. Y., Kellermann, K. I., Vermeulen, R. C., Cohen, M. H., Zensus, J. A., Ros, E. & Kardashev, N. S. 2004, submitted to *Astron. J.*
- Lister, M. L., Tingay, S. J. Murphy, D. W., Piner, B. G., Jones, D. L. & Preston, R. A., 2001, *ApJ*, 554, L948
- Lister, M. L, Tingay, S. J. & Preston, R. A. 2001, *ApJ*, 554, 964
- Lobanov, A. P. & Zensus, J. A. 2001, *Science*, 294, 128
- Lovell, J. E. J., et al. 2000, in *Proceedings of the VSOP Symposium, January 2000, Astrophysical Phenomena Revealed by Space VLBI*, ed H. Hirabayashi, P. G. Edwards, & D. W. Murphy (Sagamihara: The Institute of Space and Astronautical Science), 183
- Lovell, J. E. J. et al. 2004, submitted to *ApJ Supp.* (Paper II)
- Lovell, J. E. J., Jauncey, D. L., Bignall, H. E., Kedziora-Chudczer, L., Macquart, J-P, Rickett, B. J. & Tzioumis, A. K. 2003 *AJ*, 126, 1699
- Melrose, D. B. 2002, *Publ. Astron. Soc. Aust.* 2002, 19, 34
- Moellenbrock, G. A., et al. 1996, *AJ*, 111, 2174
- Moellenbrock, G. A., et al. 2000, in *Proceedings of the VSOP Symposium, January 2000, Astrophysical Phenomena Revealed by Space VLBI*, ed H. Hirabayashi, P. G. Edwards, & D. W. Murphy (Sagamihara: The Institute of Space and Astronautical Science), 177
- Murphy, D. W., Preston, R. A. & Hirabayashi, H. 2003, *New Astronomy Reviews*, 47, 633
- Piner, B.G., Edwards, P.G., Wehrle, A.E., Hirabayashi, H., Lovell, J.E.J. & Unwin, S.C. 2000, *ApJ*, 537, 91
- Readhead, A. C. S., Taylor, G. B., Xu, W. & Pearson, T. J. 1996, *ApJ*. 460, 612
- Scott, W. K. et al. , 2004, submitted to *ApJ Supp.* (Paper III).
- Shklovsky, I. S. 1963, *Sov. Astron.*, 6, 465
- Sincell, M. W. & Krolik, J. H. 1994, *ApJ*, 430, 550
- Tingay, S. J. et al., 2001, *ApJ*, 549, L55
- Tingay, S. J. et al. 2002, *ApJ Suppl*, 141, 311

Tingay, S. J., Jauncey, D. L., King, A. K.,
Tzioumis, A. K., Lovell, J. E. J. & Edwards,
P. G., 2003, PASJ, 44, 351

Vermeulen, R. C. & Cohen, M. H. 1994, ApJ 430,
467

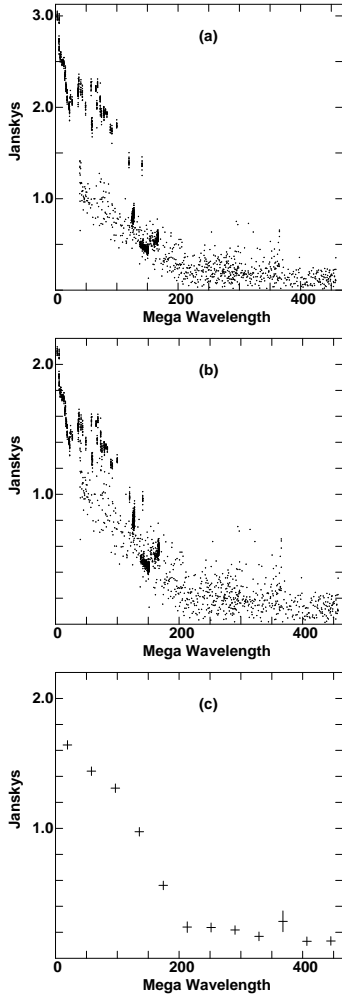


Fig. 1.— **Combining and Averaging the VSOP and VLBA Data:** (a): The visibility amplitude versus the projected spacing (u,v) is shown for the source J1626–2951. The VSOP data at the longer spacings are shown by the fainter dots; the VLBA data at the shorter spacings are shown by the darker dots. These observations were taken nearly two years apart. (b): The same plot as in (a) after correcting the VLBA amplitude scale, based on the measured variability of the source. (c): Each point shows the average visibility amplitude and error estimate for all data within each interval of 40 M λ projected spacing.

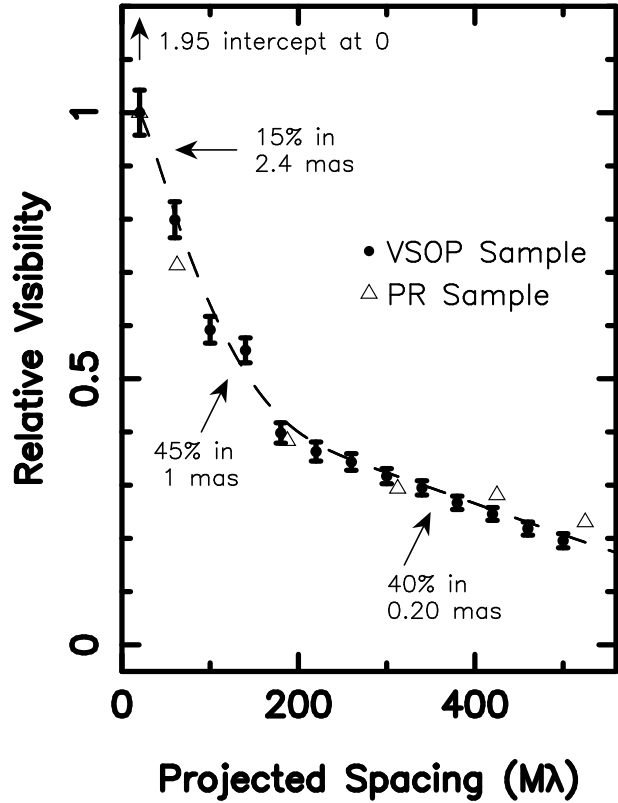


Fig. 2.— **The Relative Visibility versus Projected Spacing for the VSOP AGN Sample:** The relative visibility distribution, normalized to 1.0 at 20 M λ , is shown by the plotted solid points. The error estimate is based on the number of sources compiled for each point. The distribution for the Pearson-Readhead sample of 24 sources is given by the open triangles. The dashed line shows the dependence of the relative visibility for a three component model with component sizes and proportions as indicated. Each spacing bin is 40 M λ wide and not all bins were sampled for all sources. The maximum resolution for a source observed with VSOP varied between 300 to 540 M λ , the maximum resolution for VLBA observations was 150 M λ . At zero spacing, the average visibility is 1.95 times that at 20 M λ . A spacing of 500 M λ corresponds to 25,000 km.

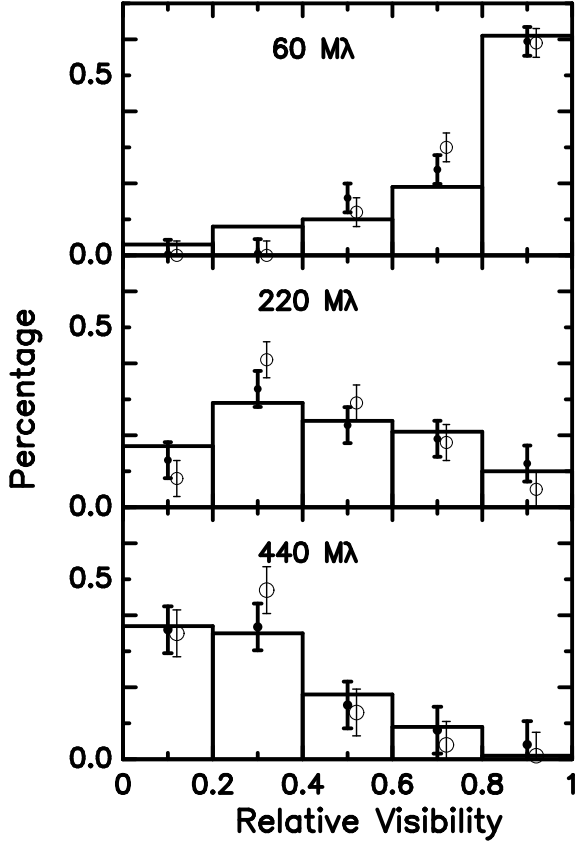


Fig. 3.— **The Fit to the Relative Visibility Distributions Versus Spacing:** The histogram of the relative visibility for the sources in the sample are given for the three indicated spacings. The plotted points show the distribution from the template source model convolved with a core angular-size distribution shown in Fig. 3, using the parameters of Eq.(1). The error bars are estimated from the number of observations at each resolution. The lighter plotted points show a relatively poor fit associated with a model with a larger core diameter (see text).

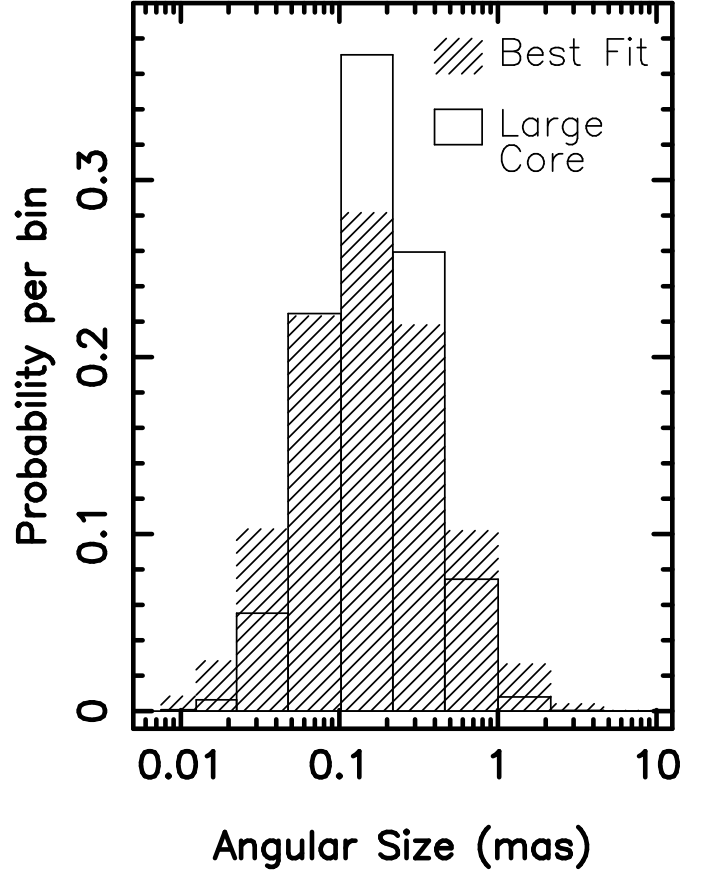


Fig. 4.— **The Derived Core Angular-Size Distributions:** The probability distribution of the core angular size distribution with $\theta_l = 0.052$ mas and $d = 1.45$ (see Eq. (1)) is shown by the cross-hatched histogram, correspond to the darker plotted points in Fig. 3. The open histogram shows the distribution associated with the model for a larger core, $\theta_l = 0.09$ mas and $d = 1.08$, shown by the lighter plotted points in Fig. 3.

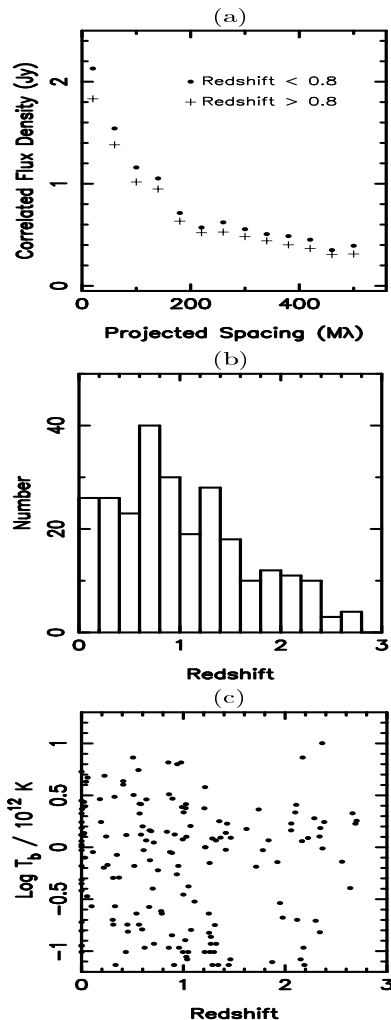


Fig. 5.— (a) The Correlated Flux Density versus Projected Spacing for Sources in the Sample: This plot is similar to Fig. 2, but with the ordinate values in correlated flux density, rather than normalized to 1.0 at $20 M\lambda$. The sample was split into two nearly equal parts, defined by the source redshift. The higher redshift sample has about 15% less flux density at all spacings than the lower redshift sample. (b) **The Distribution of redshift:** The number distribution for the 277 of the 303 sources in the sample with a measured redshift. (c) **The Dependence of the Brightness Temperature with Redshift:** The approximate brightness temperatures, given in Table 1, Col (8) is plotted versus redshift if available. Little core flux density versus redshift is observe; hence, the correction from the observer’s frame to the source frame by simply increasing the brightness temperature scale by 1.81 is valid.

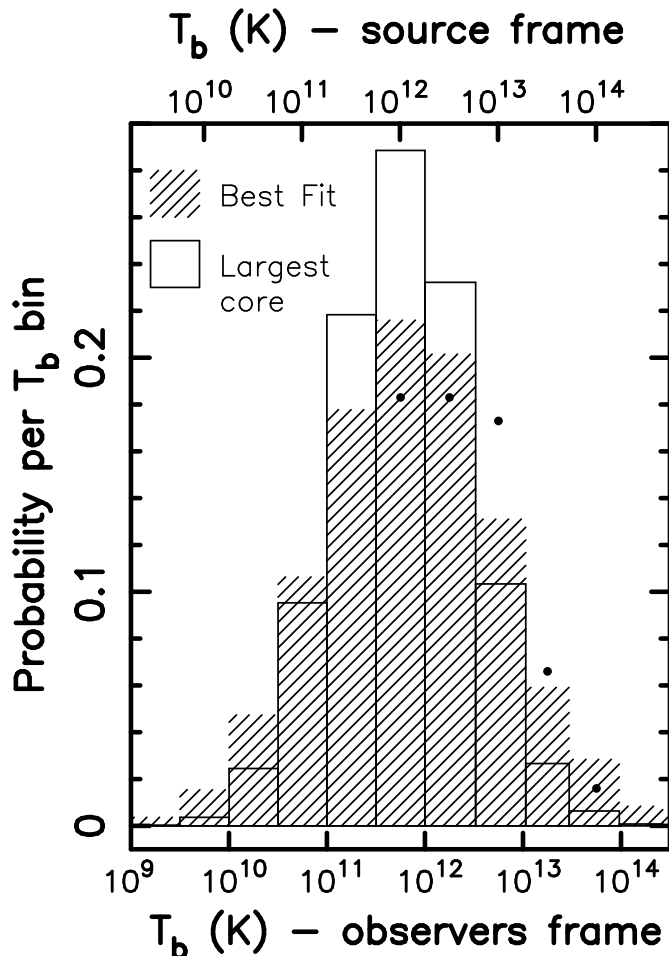


Fig. 6.— **The Brightness Temperature Distributions of the VSOP AGN Sample:** The brightness temperature distribution, implied by the core-angular size distributions, shown in Fig. 3. The cross-hatched distribution is the best fit to the VSOP AGN sample; the open distribution is for the model with the larger core size. The plotted points at the high brightness temperature tails are shown for the model discussed in the text, with $v_b/c = 0.993$, $T_{max} = 1 \times 10^{12} \text{K}$, and $\psi = 35^\circ$.

TABLE 1
VSOP AGN SURVEY SOURCE LIST

(1) IAU Name	(2) Alt Name	(3) S ₅	(4) ID	(5) z	(6) Exp	(7) Class	(8) T _b	(9) OBS _{vsop}	(10) OBS _{vlba}	(11) MOJAVE
J0006-0623	0003-066	2.5	g	0.347	vs03t	A	6.5	29-08-98	05-06-96	M
J0013+4051	0010+405	1.0	g	0.255	vs13a	B			05-06-96	
J0019+7327	0016+731	1.7	q	1.781	vs07a	A	1.9	02-03-98	02-03-98	M
J0029+3456	0025+345	1.3	g	0.600		C			05-06-96	M
J0038+4137	0035+413	1.1	q	1.353		C			05-06-96	M
J0042+2320	0039+230	1.6	e		vs07u	A	1.3	12-08-99	05-06-96	
J0105+4819	0102+480	1.1	e		vs08q	B			05-06-96	
J0106-4034	0104-408	2.6	q	0.584	vs03s	A	6.3	08-06-98	05-06-96	
J0108+0135	0106+013	3.4	q	2.099	vs02t	B			05-06-96	M
J0111+3906	0108+388	1.3	g	0.669		C			05-06-96	M
J0115-0127	0112-017	1.6	q	1.365	vs07t	A	1.4	10-08-99	05-06-96	M
J0116-1136	0113-118	1.9	q	0.672	vs06h	A	1.7	15-07-01	05-06-96	
J0119+0829	0116+082	1.2	g	0.584		C			05-06-96	
J0119+3210	0116+319	1.6	g	0.060		D			05-06-96	
J0120-2701	0118-272	1.2	b	0.559		C			05-06-96	
J0121+1149	0119+115	1.1	q	0.570	vs08p	A	0.1	22-07-01	05-06-96	M
J0121+0422	0119+041	2.0	q	0.637	vs05y	A	0.2	01-08-98	05-06-96	M
J0125-0005	0122-003	1.6	q	1.070	vs05x	A	1.3	02-08-98	05-06-96	
J0126-0123	0123-106	1.3	e			D			05-06-96	
J0126+2559	0123+257	1.4	q	2.364	vs08o	A	0.8	20-07-01	05-06-96	
J0132-1654	0130-171	1.2	q	1.022	vs08c	B			05-06-96	
J0136+4751	0133+476	2.4	q	0.859	vs03r	A	3.7	16-08-99	16-08-99	M
J0141-0928	0138-097	1.2	b	0.440	vs10i	B			05-06-96	
J0149+0555	0146+056	1.5	q	2.345	vs06z	A	1.7	27-07-01	05-06-96	
J0152+2207	0149+218	1.1	q	1.320	vs08n	B			05-06-96	M
J0153-3310	0150-334	1.4	q	0.610		C			05-06-96	
J0155-4048	0153-410	1.2	g	0.226		C			05-06-96	
J0157+7442	0153+744	1.5	q	2.338		C			05-06-96	M
J0204+1514	0202+149	2.7	q		vs03i	B			05-06-96	M
J0204-1701	0202-172	1.4	q	1.740	vs08b	B			05-06-96	
J0205+3212	0202+319	1.0	q	1.466	vs12c	B			05-06-96	M
J0217+7349	0212+735	3.2	b	2.367	vs02o	A	1.5	05-09-97	05-09-97	M
J0217+0144	0215+015	1.6	b	1.715	vs07r	A	0.1	03-08-98	05-06-96	
J0221+3556	0218+357	1.5	q	0.936		C			05-06-96	M
J0224+0659	0221+067	1.0	q	0.511	vs12b	B			05-06-96	M
J0226+3421	0223+341	1.7	q		vs05o	B			05-06-96	
J0231+1322	0229+131	2.4	q	2.059	vs04l	A	2.1	13-08-99	05-06-96	
J0237+2848	0234+285	3.4	q	1.213	vs02s	B			05-06-96	M
J0238+1636	0235+164	1.9	b	0.940		C			05-06-96	M
J0239+0416	0237+040	1.1	q	0.978	vs11i	B			05-06-96	
J0240-2309	0237-233	3.6	q	2.225		C			05-06-96	M
J0241-0815	NGC1052	3.2	g	0.0049		C			05-06-96	
J0242+1101	0239+108	1.6	q		vs05w	B			05-06-96	
J0251+4315	0248+430	1.4	q	1.310	vs07q	A	1.1	15-02-99	15-02-99	
J0259+0747	0256+075	1.0	b	0.893	vs12a	B			05-06-96	
J0312+0133	0310+013	1.0	q	0.664	vs11z	B			05-06-96	M
J0318+4151	NGC1265	1.5	g	0.025		D			05-06-96	
J0319+4130	3C84	42.4	g	0.0175	vs01c	A	1.2	25-08-98	25-08-98	
J0321+1221	0319+121	1.6	q	2.662	vs07p	A	2.1	14-02-01	05-06-96	

TABLE 1—*Continued*

(1) IAU Name	(2) Alt Name	(3) S ₅	(4) ID	(5) z	(6) Exp	(7) Class	(8) T _b	(9) OBS _{vsop}	(10) OBS _{vlba}	(11) MOJAVE
J0336+3218	NRAO140	2.0	q	1.258	vs05f	B			05-06-96	M
J0339-0146	CTA26	3.0	q	0.852	vs03q	A	1.4	17-02-02	05-06-96	M
J0348-2749	0346-279	1.4	q	0.987	vs08m	A	1.3	09-08-01	05-06-96	
J0402-3147	0400-319	1.0	q		vs11y	B			05-06-96	
J0403+2600	0400+258	1.0	q	2.109	vs11x	B			05-06-96	
J0403-3605	0402-362	2.2	q	1.417	vs03z	A	0.1	30-07-98	05-06-96	
J0405-1308	0403-132	3.2	q	0.571	vs03e	A	2.3	19-08-98	05-06-96	
J0406-3826	0405-385	1.3	q	1.285	vs07o	B			15-09-99	M
J0412+2305	0409+229	1.0	q	1.215		C			05-06-96	
J0414+3418	0411+341	1.6	e			C			05-06-96	
J0414+0534	0411+054	1.1	q	2.639		C			05-06-96	
J0423-0120	0420-014	4.4	q	0.915	vs02g	A	2.3	04-02-99	04-02-99	M
J0424-3756	0422-380	1.7	q	0.782	vs06y	B			05-06-96	
J0424+0036	0422+004	1.5	b	0.310	vs07z	A	2.6	24-08-99	05-06-96	
J0428-3756	0426-380	1.8	b	1.030	vs05e	B			05-06-96	
J0431+2037	0428+205	2.8	g	0.219		C			05-06-96	
J0433+0521	3C120	3.8	g	0.0329	vs02n	A	1.3	11-02-99	11/02/99	M
J0437-1844	0434-188	1.2	q	2.702	vs09m	B			05-06-96	
J0449+1121	0446+112	1.0	g	1.207	vs10h	B			05-06-96	
J0453-2807	0451-282	2.5	q	2.559	vs04g	A	4.0	12-09-99	05-06-96	
J0455-3006	0453-301	1.5	g			D			05-06-96	
J0457-2324	0454-234	2.0	b	1.003	vs05n	A	1.5	27-02-02	05-06-96	
J0459+0229	0457+024	1.7	q	2.384	vs05m	B			05-06-96	
J0501-0159	0458-020	3.3	q	2.286	vs02z	A	1.2	22-09-99	05-06-96	M
J0503+0203	0500+019	2.1	q	1.000	vs04a	B			05-06-96	
J0508+8432	0454+844	1.1	b	0.112	vs11h	B			05-06-96	
J0509+0541	0506+056	1.0	e		vs11w	B			05-06-96	
J0530+1331	0528+134	6.2	q	2.060	vs01o	B			05-06-96	M
J0532+0732	0529+075	2.0	e			C			05-06-96	
J0539-2839	0537-286	1.2	q	3.104	vs10g	A	1.4	01-10-99	05-06-96	
J0541-0541	0539-057	1.2	q	0.839	vs07y	B			05-06-96	
J0607+6720	0602+673	1.0	q		vs11v	B			05-06-96	M
J0607-0834	0605-085	2.4	q	0.870	vs03p	A	0.4	14-01-99	05-06-96	M
J0609-1542	0607-157	4.2	q	0.324	vs02a	A	0.9	04-04-98	05-06-96	
J0614+6046	0609+607	1.1	q	2.690	vs10f	B			05-06-96	
J0616-3456	0614-349	1.4	g	0.329		D			05-06-96	
J0620-3711	0618-371	1.4	g	0.033		D			05-06-96	
J0626+8202	0615+820	1.0	q	0.710	vs11u	B			18-09-99	M
J0627-3529	0625-354	2.2	g	0.055		C			05-06-96	
J0644-3459	0642-349	1.0	q	2.165	vs10e	B			05-06-96	
J0646+4451	0642+449	1.7	q	3.396	vs05l	B			23-06-99	M
J0648-3044	0636-306	1.0	q	0.455	vs11t	B			05-06-96	
J0713+4349	0710+439	1.6	q	0.518	vs06p	B			05-06-96	M
J0714+3534	0711+356	1.0	q	1.620	vs09k	A	1.4	09-04-99	09-04-99	
J0738+1742	0735+178	2.2	b	0.410	vs05d	A	1.2	30-01-99	30-01-99	M
J0739+0137	0736+017	1.8	q	0.191	vs05c	A	2.1	03-04-99	05-06-96	M
J0741+3112	0738+313	3.4	q	0.635	vs02k	A	3.2	10-01-99	10-01-99	M
J0745+1011	0742+103	3.5	e		vs02j	B			05-06-96	M
J0745-0044	0743-006	2.0	b	0.994	vs04f	B			05-06-96	

TABLE 1—*Continued*

(1)	(2)	(3)	(4)	(5)	(6)	(7)	(8)	(9)	(10)	(11)
IAU Name	Alt Name	S ₅	ID	z	Exp	Class	T _b	OBS _{vsop}	OBS _{vlba}	MOJAVE
J0748+2400	0745+241	1.2	q	0.410	vs10d	A	0.6	09-02-99	05-06-96	M
J0750+1231	0748+126	1.9	q	0.889	vs04k	B			05-06-96	M
J0758+3747	NGC2484	1.0	g	0.043		C			05-06-96	
J0808-0751	0805-077	1.6	q	1.837		C			05-06-96	
J0808+4950	0804+499	1.2	q	1.430	vs09j	B			05-06-96	M
J0811+0146	0808+019	1.5	b		vs07n	A	1.6	07-01-99	07-01-99	M
J0815+3635	0812+367	1.0	q	1.025	vs10c	B			05-06-96	
J0818+4222	0814+425	1.9	b	0.0257	vs06g	A	1.7	24-04-99	24-04-99	M
J0820-1258	0818-128	1.0	b		vs11s	B			05-06-96	
J0823+2223	0820+225	1.6	b	0.951		C			05-06-96	
J0824+5552	0820+560	1.2	q	1.417	vs09i	A	1.6	15-10-00	05-06-96	
J0824+3916	0821+394	1.0	q	1.216	vs10b	B			05-06-96	
J0825+0309	0823+033	1.6	b	0.506	vs05v	A	0.4	28-04-99	05-06-96	M
J0831+0429	0829+046	2.1	b	0.180	vs05k	B			05-06-96	M
J0834+5534	0831+557	5.8	g	0.242		C			05-06-96	
J0840+1312	0838+133	1.3	q	0.684	vs09h	B			05-06-96	
J0841+7053	0836+710	2.4	q	2.172	vs04e	A	2.7	07-10-97	07-10-97	M
J0842+1835	0839+187	1.0	q	1.270	vs10a	B			05-06-96	
J0854+5757	0850+581	1.2	q	1.322	vs09z	B			05-06-96	M
J0854+2006	OJ287	2.7	b	0.306	vs03y	A	2.9	04-04-99	04-04-99	
J0900-2808	0858-279	3.6	q	2.152		C			05-06-96	
J0903+4651	0859+470	1.3	q	1.462	vs09g	A	1.1	14-02-99	14-02-99	
J0909+0121	0906+015	1.0	q	1.018	vs11r	A	1.0	09-01-99	05-06-96	M
J0920+4441	0917+449	1.2	q	2.180	vs07x	A	3.0	07-02-99	07-02-99	M
J0921-2618	0919-260	2.3	q	2.300	vs04s	B			05-06-96	
J0921+6215	0917+624	1.5	q	1.446	vs06f	B			05-06-96	
J0927+3902	4C39.25	11.2	q	0.699	vs01f	A	2.6	23-10-97	23-10-97	M
J0948+4039	0945+408	1.6	q	1.252	vs05u	B			05-06-96	M
J0956+2515	0953+254	1.3	q	0.712	vs07l	B			05-06-96	M
J0957+5522	0954+556	2.3	q	0.909		D			05-06-96	
J0958+4725	0955+476	1.3	q	1.873	vs07k	B			05-06-96	
J0958+6533	0954+658	1.4	b	0.368	vs08k	B			05-06-96	
J1006+3454	3C236	1.7	g	0.0989		D			05-06-96	
J1014+2301	1012+232	1.1	q	0.565	vs11g	B			05-06-96	M
J1018-3144	1015-314	1.8	q	1.346		D			05-06-96	
J1035-2011	1032-199	1.1	q	2.189	vs11f	A	1.7	21-02-98	05-06-96	M
J1035+5628	1031+567	1.3	g	0.450		C			05-06-96	
J1037-2934	1034-293	1.6	b	0.312	vs05t	A	2.8	02-06-99	02-06-99	
J1041+0610	1038+064	1.7	q	1.270	vs05j	B			05-06-96	
J1042+1203	3C245	1.7	q	1.029		C			05-06-96	
J1044+8054	1039+811	1.1	q	1.260	vs11e	B			05-06-96	
J1048-1909	1045-188	1.1	q	0.595	vs11d	B			05-06-96	
J1048-4114	1045-188	1.0	q	0.620		C			05-06-96	
J1051-3138	1048-313	1.0	e		vs09y	A	0.1	20-05-99	05-06-96	
J1051+2119	1049+215	1.3	q	1.300	vs07j	B			05-06-96	M
J1058+0133	1055+018	4.1	b	0.888	vs02l	A	7.3	12-05-99	12-05-99	M
J1058+1951	1055+201	1.7	q	1.110	vs06x	B			05-06-96	M
J1118+1234	1116+128	2.0	q	2.118	vs05s	A	1.0	17-12-97	05-06-96	
J1125+2610	1123+264	1.1	q	2.341	vs09f	B			05-06-96	M

TABLE 1—*Continued*

(1) IAU Name	(2) Alt Name	(3) S ₅	(4) ID	(5) z	(6) Exp	(7) Class	(8) T _b	(9) OBS _{vsop}	(10) OBS _{vlba}	(11) MOJAVE
J1127–1857	1124–186	1.6	q	1.050	vs07i	B			05-06-96	M
J1146–2447	1143–245	1.5	q	1.950	vs06w	A	4.2	26-05-99	05-06-96	
J1146–3328	1143–331	1.1	g			C			05-06-96	
J1147–3812	1144–379	2.2	b	1.048	vs04d	A	0.2	28-12-97	05-06-96	
J1147–0724	1145–071	1.2	q	1.342	vs09x	A	1.5	08-03-00	05-06-96	M
J1150–0023	1148–001	2.0	q	1.976	vs05r	B			05-06-96	M
J1153+4931	1150+497	1.0	q	0.334	vs09w	B			05-06-96	
J1153+8058	1150+812	1.4	q	1.250	vs06v	B			05-06-96	
J1158+2450	1155+251	1.2	g			C			05-06-96	M
J1159+2914	1156+295	1.8	q	0.729	vs05b	B			05-06-96	M
J1205–2634	1203–262	1.1	q	0.789	vs11c	B			05-06-96	
J1209–2406	1206–238	1.1	q		vs11b	B			05-06-96	
J1215–1731	1213–172	1.8	g		vs05a	A	0.9	11-01-98	05-06-96	
J1215+3448	1213+350	1.1	q	0.857		C			05-06-96	
J1219+4829	1216+487	1.0	q	1.076	vs11a	B			05-06-96	
J1224+0330	1222+037	1.2	q	0.957	vs09e	B			05-06-96	
J1224+2122	1222+216	1.4	q	0.435	vs06o	B			05-06-96	
J1225+1253	3C272.1	3.6	g	0.0033		D			05-06-96	
J1229+0203	3C273B	43.6	q	0.1583	vs01b	A	1.4	22-12-97	22-12-97	M
J1232–0224	1229–021	1.0	q	1.038		C			05-06-96	
J1239–1023	1237–101	1.3	q	0.750		C			05-06-96	
J1246–0730	1243–072	1.1	q	1.286	vs10z	B			05-06-96	
J1246–2547	1244–255	2.3	q	0.638	vs04r	A	6.5	21-01-98	05-06-96	
J1256–0547	3C279	13.0	q	0.538	vs01g	A	4.6	10-01-98	10-01-98	M
J1257–3155	1255–316	1.4	q	1.924	vs06u	A	2.1	25-05-99	05-06-96	
J1305–1033	1302–102	1.0	q	0.286	vs11q	A	1.1	07-01-98	05-06-96	M
J1309+1154	1307+121	1.3	b		vs09d	B			05-06-96	
J1310+3220	1308+326	3.6	b	0.996	vs02e	A	10.0	29-06-98	29-06-98	M
J1316–3338	1313–333	1.6	q	1.210	vs05q	A	0.6	20-01-98	05-06-96	
J1332+0200	1330+022	1.5	g	0.215		C			05-06-96	
J1337–1257	1334–127	4.4	b	0.539	vs01y	A	1.0	10-07-99	10-07-99	M
J1347+1217	1345+125	3.1	g	0.1202		C			05-06-96	M
J1351–1449	1349–145	1.1	e		vs10y	B			05-06-96	
J1354–1041	1352–104	1.0	q	0.332		C			05-06-96	
J1357+1919	1354+195	2.7	q	0.720	vs03x	A	0.3	19-07-99	05-06-96	
J1357–1744	1354–174	1.1	q	3.147	vs08j	A	1.1	30-01-98	05-06-96	
J1405+0415	1402+044	1.0	q	3.193	vs10x	B			05-06-96	
J1407+2827	OQ208	2.4	g	0.0769	vs03o	A	3.1	30-06-98	30-06-98	M
J1408–0752	1406–076	1.0	q	1.494	vs11p	B			05-06-96	
J1415+1320	1413+135	1.2	b	0.260	vs09v	B			05-06-96	M
J1419+5423	1418+546	1.7	b	0.152		C			05-06-96	
J1419–1928	1417–192	1.0	g	0.119	vs11o	B			05-06-96	
J1427–4206	1424–418	3.8	q	1.522	vs02i	B			05-06-96	
J1430+1043	1427+109	1.2	q	1.710	vs09c	A	0.6	18-01-01	05-06-96	
J1436+6336	1435+638	1.1	q	2.068	vs08i	A	1.1	21-06-01	05-06-96	
J1445+0958	1442+101	1.2	q	3.535		C			05-06-96	
J1454–3747	1451–375	2.4	q	0.314	vs03n	B			05-06-96	
J1501–3918	1458–391	1.2	g	1.083		C			05-06-96	
J1504+1029	1502+106	1.8	q	1.839	vs04z	A	2.5	27-07-00	05-06-96	M

TABLE 1—*Continued*

(1) IAU Name	(2) Alt Name	(3) S ₅	(4) ID	(5) z	(6) Exp	(7) Class	(8) T _b	(9) OBS _{vsop}	(10) OBS _{vlba}	(11) MOJAVE
J1506+3730	1504+377	1.0	g	0.674	vs10w	B			05-06-96	M
J1507-1652	1504-166	2.8	q	0.876	vs03m	A	0.5	10-04-98	05-06-96	M
J1512-0905	1510-089	3.3	q	0.360	vs02x	A	4.8	11-08-99	11-08-99	M
J1513-1012	1511-100	1.2	q	1.513	vs09u	B			05-06-96	M
J1516+0015	1514+004	1.6	g	0.0523	vs07h	A	1.3	24-08-98	05-06-96	
J1517-2422	1514-241	2.2	g	0.042	vs03u	A	1.2	27-04-98	05-06-96	M
J1522-2730	1519-273	2.3	b	1.294	vs04q	A	0.8	05-02-99	05-02-99	M
J1526-1351	1524-136	1.3	q	1.687		C			05-06-96	
J1534+0131	1532+016	1.3	q	1.435		C			05-06-96	M
J1540+1447	1538+149	1.2	b	0.605	vs09t	B			05-06-96	
J1543-0757	1540-077	1.0	g			C			05-06-96	
J1546+0026	1543+005	1.3	g	0.550	vs09b	B			05-06-96	
J1549+0237	1546+027	1.5	q	0.413	vs06e	A	2.4	31-07-98	05-06-96	M
J1550+0527	1548+056	3.3	q	1.422	vs02r	B			05-06-96	M
J1557-0001	1555+001	2.3	q	1.770	vs04p	B			05-06-96	
J1602+3326	1600+335	2.0	g		vs04y	B			05-06-96	
J1608+1029	1606+106	1.7	q	1.226	vs06s	B			05-06-96	M
J1613+3412	1611+343	4.0	q	1.401	vs02b	A	1.1	04-02-98	05-06-96	M
J1625-2527	1622-253	3.5	g	0.786	vs02h	B			05-06-96	M
J1625+4134	1624+416	1.4	q	2.550		C			05-06-96	
J1626-2951	1622-297	2.4	q	0.815	vs03l	A	0.6	22-02-98	05-06-96	
J1635+3808	1633+382	3.2	q	1.814	vs03d	A	0.6	04-08-98	04-08-98	M
J1637+4717	1636+473	1.3	q	0.740	vs09a	B			05-06-96	
J1638+5720	1637+574	1.8	q	0.745	vs06n	A	0.7	21-04-98	21-04-98	
J1640+3946	NRAO512	1.3	q	1.660	vs08y	A	0.3	03-09-99	05-06-96	M
J1640+1220	1638+124	1.3	g		vs08z	B			05-06-96	
J1642+3948	3C345	8.4	q	0.593	vs01k	A	5.5	28-07-98	28-07-98	M
J1642+6856	1642+690	1.5	q	0.751	vs07w	A	0.8	31-05-98	31-05-98	M
J1642-0621	1639-062	1.6	e		vs13m	B			05-06-96	M
J1653+3945	MARK501	1.4	b	0.0336	vs08h	A	0.7	07-04-98	07-04-98	
J1658+4737	1656+477	1.4	q	1.622	vs08g	A	0.2	28-08-99	05-06-96	
J1658+0741	1655+077	1.6	q	0.621	vs07g	A	1.7	05-03-98	05-06-96	M
J1658+0515	1656+053	2.1	q	0.879	vs05i	A	1.2	04-03-98	05-06-96	M
J1658-0739	1656-075	1.3	q	3.700		C			05-06-96	
J1710+0036	1708+006	1.1	g			D			05-06-96	
J1727+4530	1726+455	1.3	q	0.714	vs07f	B			05-06-96	
J1728+0427	1725+044	1.2	q	0.296		C			05-06-96	
J1733-1304	NRAO530	7.0	q	0.902	vs01m	A	2.6	08-09-97	05-06-96	M
J1734+3857	1732+389	1.3	b	0.970	vs07e	B			05-06-96	
J1740+5211	1739+522	1.1	q	1.375	vs10v	A	4.3	14-06-98	14-06-98	M
J1743-0350	1741-038	2.4	q	1.054	vs03k	B			05-06-96	M
J1745-0753	1742-078	1.4	e			C			05-06-96	
J1751+0939	1749+096	2.3	b	0.322	vs04o	A	0.7	20-08-98	20-08-98	M
J1753+4409	1751+441	1.0	q	0.871	vs11n	B			05-06-96	
J1800+7828	1803+784	2.6	b	0.680	vs02w	A	0.9	16-10-97	16-10-97	M
J1801+4404	1800+440	1.1	q	0.663	vs10u	B			05-06-96	
J1804+0101	1801+010	1.6	q	1.522		C			05-06-96	
J1806+6949	3C371	2.2	b	0.051	vs04x	A	5.3	11-03-98	11-03-98	
J1824+1044	1821+107	1.1	q	1.360	vs10t	B			05-06-96	

TABLE 1—*Continued*

(1) IAU Name	(2) Alt Name	(3) S ₅	(4) ID	(5) z	(6) Exp	(7) Class	(8) T _b	(9) OBS _{vsop}	(10) OBS _{vlba}	(11) MOJAVE
J1824+5651	1823+568	1.5	b	0.664	vs06d	A	0.6	31-05-98	31-05-98	M
J1832+2833	1830+285	1.1	q	0.594	vs10s	B			05-06-96	
J1902+3159	3C395	1.9	q	0.635	vs06c	A	1.2	01-05-98	01-05-98	M
J1911-2006	1908-201	2.3	e		vs04n	B			05-06-96	
J1924-2914	1921-293	14.8	q	0.352	vs01e	A	1.4	19-06-98	19-06-98	M
J1927+7358	1928+738	3.6	q	0.303	vs02m	A	2.1	22-08-97	05-06-96	M
J1937-3958	1933-400	1.1	q	0.966	vs08f	B			05-06-96	
J1949-1957	1946-200	1.3	e		vs13c	B			05-06-96	
J1955+5131	1954+513	3.1	q	1.220	vs13d	B			05-06-96	M
J1957-3845	1954-388	4.4	q	0.630	vs01x	B			05-06-96	
J2000-1748	1958-179	1.8	q	0.650	vs04w	A	2.4	25-06-98	05-06-96	
J2003-3251	2000-330	1.2	q	3.773	vs08x	B			05-06-96	
J2005+7752	2007+777	1.7	b	0.342	vs06r	A	1.0	10-03-98	10-03-98	M
J2011-1546	2008-159	1.4	q	1.180	vs07d	A	0.8	25-10-97	05-06-96	
J2022+6136	2021+614	3.0	q	0.227	vs02q	A	1.1	06-11-97	06-11-97	M
J2031+1219	2029+121	1.2	b	1.215	vs08w	B			05-06-96	
J2101+0341	2059+034	1.3	q	1.105	vs08v	A	0.9	14-11-00	05-06-96	
J2109-4110	2106-413	2.3	q	1.055	vs03w	B			05-06-96	
J2110-1020	2107-105	1.2	q		vs09r	B			05-06-96	
J2115+2933	2113+293	1.2	q	1.514	vs09q	B			05-06-96	M
J2123+0535	2121+053	3.2	q	1.878	vs03c	B			05-06-96	M
J2129-1538	2126-158	1.2	q	3.268	vs08e	A	1.6	13-07-98	13-07-98	
J2131-1207	2128-123	3.0	q	0.501	vs13e	B			05-06-96	M
J2136+0041	2134+004	12.4	q	1.392	vs01h	A	1.3	28-11-97	05-06-96	M
J2139+1423	2136+141	2.0	q	2.427	vs04c	A	2.9	25-08-98	05-06-96	M
J2147+0929	2144+092	1.1	q	1.113	vs10r	B			05-06-96	M
J2148+0657	2145+067	6.4	q	0.990	vs01l	B			05-06-96	M
J2151+0552	2149+056	1.0	g	0.740	vs10q	B			05-06-96	
J2151-3027	2149-306	1.4	q	2.345		C			05-06-96	
J2158-1501	2155-152	3.1	b	0.672	vs03g	A	1.2	15-08-98	05-06-96	M
J2202+4216	BLLAC	5.6	b	0.0686	vs01q	A	2.8	08-12-97	08-12-97	M
J2203+3145	2201+315	2.9	q	0.301	vs13f	B			05-06-96	M
J2206-1835	2203-188	4.3	q	0.619		D			05-06-96	
J2212+2355	2209+236	1.4	q		vs06l	A	2.3	27-05-98	05-06-96	M
J2213-2529	2210-257	1.0	q	1.833	vs13h	B			05-06-96	
J2218-0335	2216-038	2.7	q	0.901	vs03j	A	0.9	03-12-97	05-06-96	
J2225+2118	2223+210	1.2	q	1.959		C			05-06-96	
J2225-0457	3C446	6.4	b	1.404	vs01s	A	1.6	02-12-00	05-06-96	M
J2229-0832	2227-088	2.4	q	1.561	vs04i	A	1.3	27-11-97	05-06-96	M
J2230+6946	2229+695	1.4	g			C			05-06-96	M
J2236+2828	2234+282	1.6	q	0.795	vs07c	A	0.3	24-07-99	05-06-96	
J2243-2544	2240-260	1.2	b	0.774		C			05-06-96	
J2246-1206	2243-123	2.7	q	0.630	vs03v	A	2.3	03-06-98	05-06-96	M
J2249+1136	NGC7385	1.1	g	0.026		D			05-06-96	
J2250+1419	2247+140	1.2	q	0.237		D			05-06-96	
J2253+1608	3C454.3	16.0	q	0.859	vs01d	A	0.7	12-12-97	12-12-97	M
J2255+4202	2253+417	1.1	q	1.476	vs13g	B			05-06-96	
J2258-2758	2255-282	2.5	q	0.926	vs03f	B			05-06-96	M
J2311+3425	2308+341	1.0	q	1.817	vs13n	B			05-06-96	

TABLE 1—*Continued*

(1)	(2)	(3)	(4)	(5)	(6)	(7)	(8)	(9)	(10)	(11)
IAU Name	Alt Name	S ₅	ID	z	Exp	Class	T _b	OBS _{vsop}	OBS _{vlba}	MOJAVE
J2320+0513	2318+049	1.2	q	0.623	vs09p	A	1.3	08-12-00	05-06-96	M
J2321+2732	2319+272	1.0	q	1.253	vs13i	B			05-06-96	
J2330+1100	2328+107	1.2	q	1.489	vs13j	B			05-06-96	
J2331–1556	2329–162	1.9	q	1.155	vs06b	A	0.5	11-06-98	05-06-96	
J2333–2343	2331–240	1.1	g	0.0477		C			05-06-96	
J2346+0930	2344+092	1.4	q	0.677	vs13k	B			05-06-96	
J2354+4553	2351+456	1.2	q	1.992	vs13l	B			05-06-96	
J2357–1125	2354–116	1.4	q	0.960	vs13l	B			05-06-96	
J2358–1020	2355–106	1.6	q	1.622	vs06k	A	0.4	10-12-00	05-06-96	

NOTE.—Column (7): A=AGN sample and observed with VSOP; B=AGN sample, but not yet observed with VSOP or reduced; C=AGN sample, but too faint to be observed with VSOP; D=Removed from AGN sample. Redshift and identification for J1501–3918 and J1658–0739 from I.A.G. Snellin & P.G. Edwards (2004, private communication); redshift for J1522–2730 from Heidt et al. (2004)